nanoenergy advances

Article

Ultrathin, Stretchable, and Twistable Ferroelectret Nanogenerator for Facial Muscle Detection

Ziling Song [1,†], Xianfa Cai [1,†], Zhi Chen [1], Ziying Zhu [2], Yunqi Cao [2] and Wei Li [1,3,*]

[1] College of Integrated Circuit Science and Engineering, Nanjing University of Posts and Telecommunications, 9 Wenyuan Rd., Nanjing 210046, China; jxndsongziling@outlook.com (Z.S.); xianfacai@njupt.edu.cn (X.C.); zhi.chnee@gmail.com (Z.C.)
[2] College of Control Science and Engineering, Zhejiang University, Hangzhou 310027, China; zhuziying@zju.edu.cn (Z.Z.); caoyunqi@zju.edu.cn (Y.C.)
[3] Department of Mechanical Engineering, University of Vermont, 33 Colchester Ave., Burlington, VT 05405, USA
* Correspondence: wei.li@uvm.edu
† These authors contributed equally to this work.

Abstract: Ferroelectret nanogenerators (FENGs) have garnered attention due to their unique porous structure and excellent piezoelectric performance. However, most existing FENGs lack sufficient stretchability and flexibility, limiting their application in the field of wearable electronics. In this regard, we have focused on the development of an ultrathin, stretchable, and twistable ferroelectret nanogenerator (UST-FENG) based on Ecoflex, which is made up of graphene, Ecoflex, and anhydrous ethanol, with controllable pore shape and density. The UST-FENG has a thickness of only 860 µm, a fracture elongation rate of up to 574%, and a Young's modulus of only 0.2 MPa, exhibiting outstanding thinness and excellent stretchability. Its quasi-static piezoelectric coefficient is approximately 38 pC/N. Utilizing this UST-FENG device can enable the recognition of facial muscle movements such as blinking and speaking, thereby helping to monitor people's facial conditions and improve their quality of life. The successful application of the UST-FENG in facial muscle recognition represents an important step forward in the field of wearable systems for the human face.

Keywords: ferroelectret nanogenerator; stretchable; ultrathin; twistable; Ecoflex; controlled piezoelectric effect; facial muscle detection

check for updates

Citation: Song, Z.; Cai, X.; Chen, Z.; Zhu, Z.; Cao, Y.; Li, W. Ultrathin, Stretchable, and Twistable Ferroelectret Nanogenerator for Facial Muscle Detection. *Nanoenergy Adv.* **2024**, *4*, 344–354. https://doi.org/10.3390/nanoenergyadv4040021

Academic Editors: Christian Falconi and Ya Yang

Received: 31 July 2024
Revised: 6 October 2024
Accepted: 1 November 2024
Published: 15 November 2024

1. Introduction

With the rapid development of the Internet of Things (IoT) and artificial intelligence, ferroelectret nanogenerators (FENGs) have received wide attention as a potential flexible electronic material [1–3]. An FENG is a polymer thin film with unique cellular structure and an internal quasi-permanent dipole moment that can exhibit macroscopic piezoelectric effects [4–6]. Since scientists discovered that porous polypropylene (PP) thin films have excellent piezoelectric properties, much research has focused on their preparation, performance characterization, theoretical model establishment, and application development [7–9].

One of the characteristics of ferroelectrets is that they can bind the charge in the internal vacancies to form macroscopic dipoles during the polarization process, thereby exhibiting macroscopic piezoelectric effects [10–12]. However, most preparation methods of ferroelectrets, such as chemical foaming, are difficult to control in terms of the shape and distribution of the pores [13–15]. When the shape of the hole is irregular and the distribution is not uniform, the internal electric field distribution will be uneven during the polarization process, preventing the effective accumulation and directional arrangement of charges, thus reducing the macroscopic piezoelectric effect of the material [16]. In this case, using a laser cutting machine to cut out controlled voids is an appropriate method.

In addition, some sensors are flexible, but their stretch and expansion performance are low, which limits their applicability to certain wearable scenarios and hinders accurate real-time motion guidance. To effectively address these challenges, it is necessary to develop a wearable electronic sensor that combines self-powered capabilities, flexibility, strong stretchability, continuous availability, and wide applicability. This article reports an ultrathin, stretchable, and twistable ferroelectret nanogenerator (UST-FENG) based on Ecoflex that has the characteristics of controllable hole shape and density, which strengthens the control of the geometric shape of ferroelectrets and improves their overall performance. Moreover, with its high stretchability and flexibility, the UST-FENG is able to recognize facial muscle movements such as blinking and speaking.

Over the past few decades, common materials used in the preparation of FENGs have included polypropylene (PP), formaldehyde polyvinyl alcohol (FEP), etc., but their recycling remains a challenge [17–20]. Ecoflex, as a green material, has come to people's attention [21]. Ecoflex is a biodegradable material that helps reduce plastic pollution and decreases the extensive reliance on fossil resources [22]. In addition, it possesses superior stretchability and flexibility, making it suitable as a base material for wearable FENGs [23]. Suitable electrodes are required to possess good impedance characteristics and long-term stability. [24–26]. In this paper, commercially available graphene electrodes are used for the UST-FENG. It can be well combined with the substrate Ecoflex, and it can maintain its performance under various environmental conditions [27,28].

Due to its excellent properties and potential applications, the UST-FENG has a promising application prospect in the Internet of Things, smart homes, and other related fields. Continued research and development in this area will contribute to the advancement of ultrathin, stretchable, and twistable electronics [29].

2. Fabrication Method of UST-FENG

The UST-FENG prepared in this study is based on a biodegradable, eco-friendly flexible material, Ecoflex (T00, Guoyuan Silicone Inc., Shenzhen, China), and has a typical sandwich structure. The preparation process is as shown in Figure 1. In order to prevent the film from curling and deforming during the preparation process, a "frame" formed by cutting the polyimide (PI) film is used. During the preparation, the Ecoflex pre-polymer and a platinum catalyst as the hardener are mixed at a 1:1 ratio by weight. The mixture is poured evenly onto the PI film and then placed on a desktop spin coater (KW-4B, Sedekase Electronics Inc., Beijing, China). The film thickness is evened out at a speed of 200 rpm for 30 s, and then at a speed of 250 rpm for another 30 s. It is then cured at 135 °C for 5 min, and then the excess Ecoflex is removed using a blade, resulting in an about 200 μm thick Ecoflex flexible film. This method was used to prepare three such films, one of which served as the middle Ecoflex layer and was perforated using a laser cutting machine (SM–F10) that employs a UV laser (cold light source). We used the laser cutting machine to cut a circular array of 16 × 16 holes with a total of 256 holes in this middle Ecoflex layer, and the hole diameter was 2 mm. The surfaces of the other two films were coated with graphene to serve as flexible electrodes for the UST-FENG. To be specific, we first covered the surface of the film with a mold to keep the edge of the electrode at a certain distance from the edge of the film. Then, we poured the graphene powder evenly on the film and used a precision scraper to smooth the graphene powder to apply the graphene layer to the Ecoflex film. A 0.1 mm diameter enameled wire was used as a lead electrode, which was placed on the graphene surface, and the UST-FENG was encapsulated with polyurethane films (PU, Biyi Plus Inc., Jiangxi, China) with a thickness of 50 μm, which is a medical-grade polyurethane film to ensure that the device is not affected by the environment and suitable for contact with human skin. Finally, the three films were assembled to form the UST-FENG. As the Ecoflex and PU films have a certain degree of stickiness, the production of the UST-FENG does not require additional adhesive, reflecting the simplicity and eco-friendliness of the preparation process. The UST-FENG prepared in this study has a thickness of 860 μm and is suitable for facial wearable scenes [30].

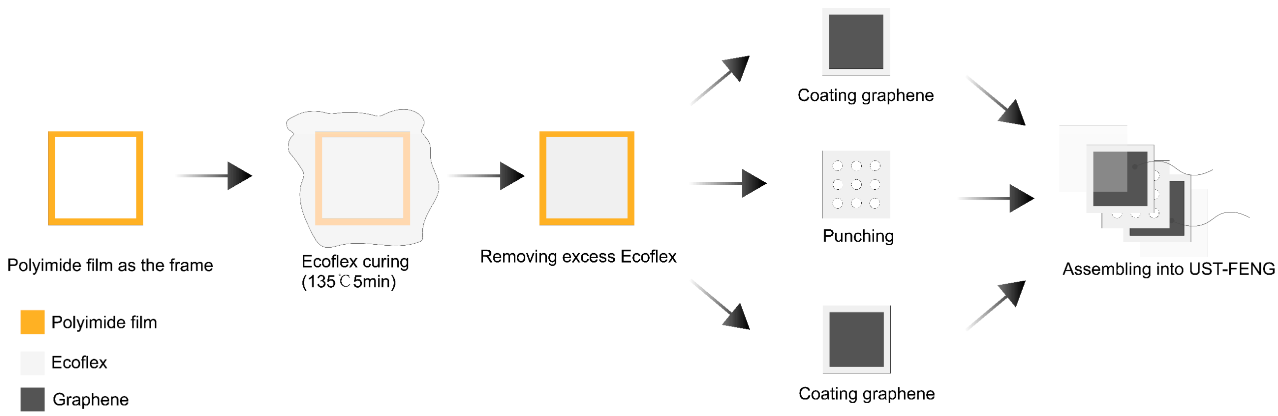

Figure 1. Preparation process of the UST-FENG.

3. Results

3.1. The Working Principle of the UST-FENG

The structure of the UST-FENG is depicted in Figure 2. The Ecoflex film, which is punched by a laser cutting machine, is located in the middle, with the upper and lower layers of Ecoflex encapsulating the bound charge. The surface of the Ecoflex is covered with graphene powder, and the outermost layers of the UST-FENG are encapsulated with PU films.

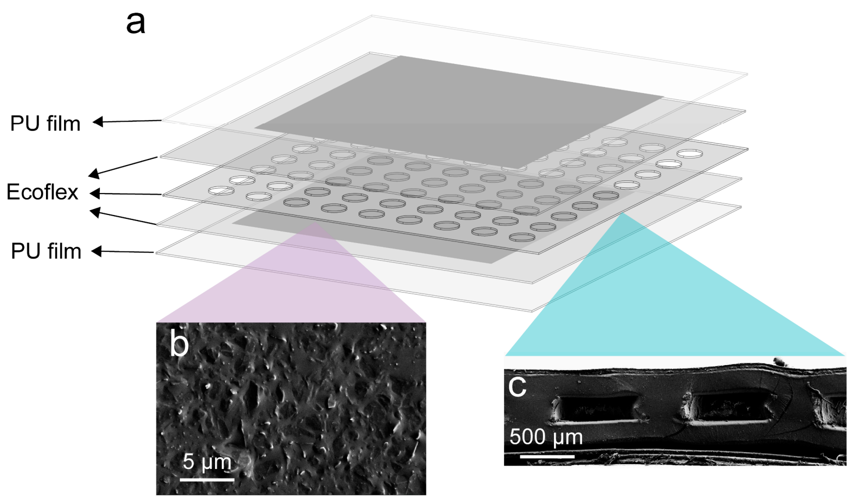

Figure 2. Structure diagram of the UST-FENG. (**a**) Structure of the UST-FENG. (**b**) SEM image of the graphene flexible electrode. (**c**) SEM image of the cross-sectional view of the UST-FENG.

The scanning electron microscope (SEM) image of the surface of the graphene electrode is shown in Figure 2b. From the figure, it is evident that the surface of the fabricated graphene electrode is densely packed and smooth. The graphene electrode developed in this study is an excellent stretchable electrode. In actual measurements, the resistance was 1.9 kΩ/cm when the electrode was not stretched and 2.5 kΩ/cm when stretched by 100%, indicating good conductivity. The superior conductivity and stability of the graphene electrode contribute to enhancing the stability of the UST-FENG's performance.

The cross-sectional view of the UST-FENG is shown in Figure 2c. It can be seen that the voids impacted by the laser cutting machine are dense and regular in shape. This shows that the UST-FENG produced in this study, as compared to those made by physical or chemical methods that randomly generate bubbles, has the advantage of stable and controllable piezoelectric performance [31,32].

The method of corona polarization is used to charge the UST-FENG [33]. During the polarization process, the corona discharge occurs when a sufficiently high voltage is applied to asymmetrical electrodes, such as needle electrodes and metal plates. The ions and excited molecules produced by corona discharge are deposited on the surface of the sample under the action of an electric field, forming a surface charge. These surface charges generate an electric field that crosses the thickness of the sample, triggering a breakdown of the gas in the void, thus charging the FENG [6]. During the deformation process of the UST-FENG under stress, the dipole moment changes, the bound charge decreases, and when the external circuit is connected, a charge flow is generated, resulting in a macroscopic piezoelectric effect [34,35].

3.2. UST-FENG Performance Simulation

The performance of the UST-FENG, which is divided into five layers, is simulated. The top and bottom layers, which are conductive electrodes, are made up of graphene. The three middle layers, also known as the sandwich layers, are composed of two layers of undrilled Ecoflex covering the upper and lower surfaces of the drilled Ecoflex film. By default, the electrode is grounded in the electrostatic field, with the charge bound to the hole's upper and lower surfaces through polarization. For the simulation, the upper and lower surfaces of the UST-FENG's hole are set to bear charges of opposite polarities. In the solid mechanics field, a fixed constraint surface is set at the geometric boundary layer where the yoz plane coincides, a roll support surface is set at the geometric boundary layer where the xoz plane coincides, and a boundary load of 4.5 kPa stress is set at the UST-FENG upper surface parallel to the xoz plane. The UST-FENG compresses under stress, releasing charge in the process. This process is simulated by coupling the electrostatic field with the solid mechanical field.

The 3D simulation results of the potential distribution are depicted in Figure 3a. The charge is concentrated on both sides of the hole, so the potential distribution primarily presents a pattern of high potential in the center and low potential around the periphery [36]. After the extrusion deformation, the charge in the middle region of the hole is effectively released, and the potential is reduced. The displacement resulting from the mechanical response is shown in Figure 3b. It represents the change in position of material points within the model. The maximum displacement at the UST-FENG boundary reaches 0.12 mm under an extrusion stress of 4.5 kPa. Figure 3c illustrates the overall stress variation at 15 times the scale factor. Figure 3d shows a cross-section of a single hole at diameter, which allows for a closer examination of the deformation in that specific area. It can be seen that the electric potential is mainly distributed on the upper and lower surfaces of the hole, and the deformation of a single hole is about 0.12 mm.

3.3. Piezoelectric Properties of UST-FENG

The UST-FENG is subjected to periodic force using a universal testing machine to characterize its longitudinal piezoelectric response. When the stress is applied to the UST-FENG, the dipole moment changes and charge flow occurs, resulting in an open-circuit voltage signal. The UST-FENG is centrally placed on a compression plate wrapped with insulating tape, and the open-circuit voltage generated is measured, as shown in Figure 4a,b. Figure 4c,d depict the voltage signals generated by the UST-FENG under vertical force. The peak force applied to the UST-FENG is approximately 65 N. When rapidly compressed, the open-circuit voltage amplitude surges, with a peak output voltage signal of 1.5 V; conversely, upon the release of external force, similar signal changes occur, but with the opposite sign. In particular, as the stress is released, the material undergoes a relaxation process, causing the waveform to oscillate. This behavior is akin to piezoelectric devices, although this effect is caused by engineered dipoles within the material rather than the material's inherent natural dipoles [37]. When the polarity of the signal acquisition electrode is switched, the voltage generated by the UST-FENG reverses [38]. This characteristic confirms that the measured output signal comes from the UST-FENG, not from artifacts caused by the measuring instrument itself.

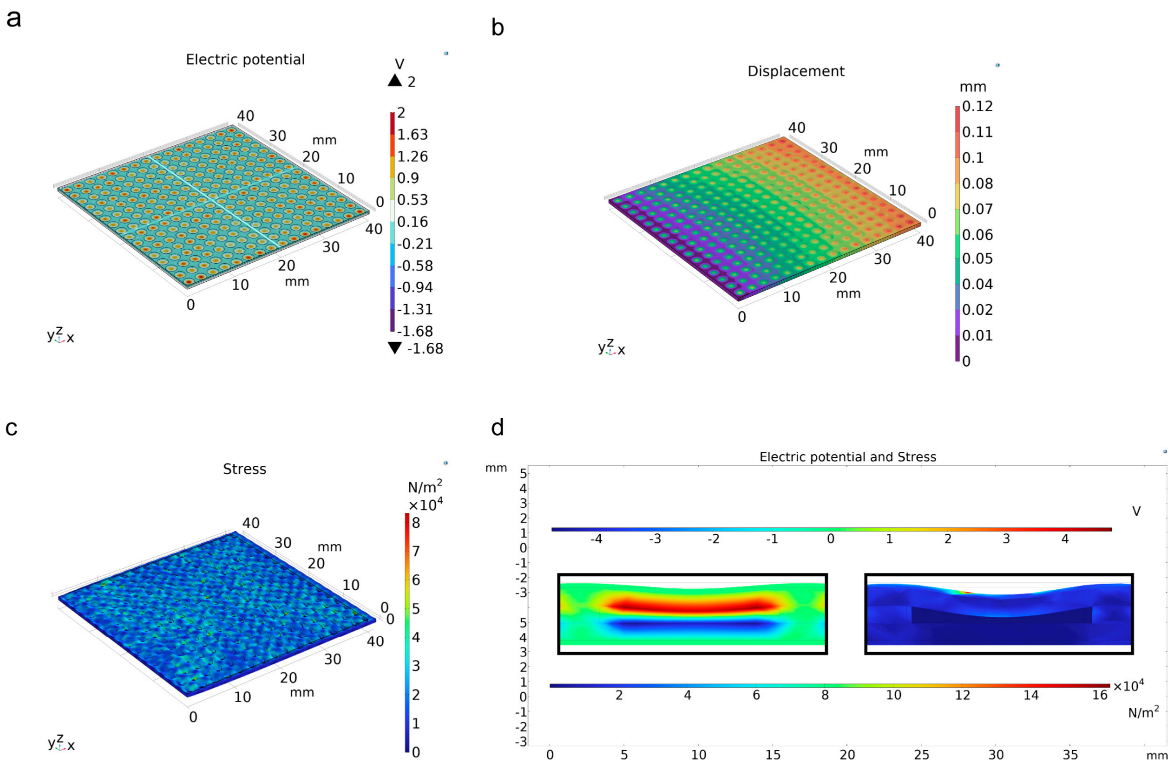

Figure 3. Simulation of the UST-FENG performance. (**a**) Potential distribution diagram of the UST-FENG. (**b**) Displacement change diagram of the UST-FENG after stress application. (**c**) Stress distribution diagram of the UST-FENG. (**d**) Cross-section diagram of the electric potential and stress distribution of the UST-FENG.

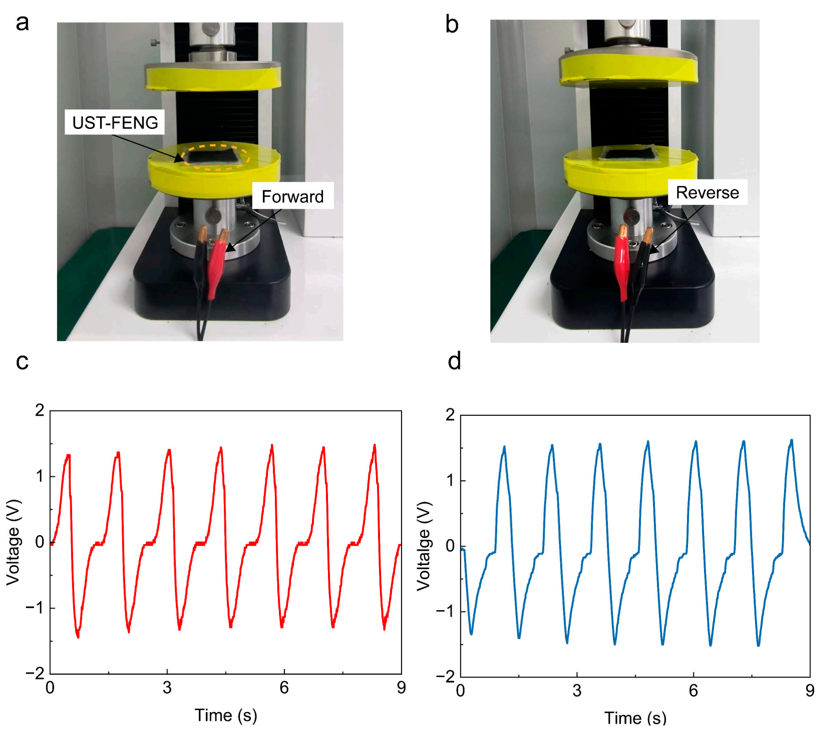

Figure 4. Piezoelectric signals generated by the UST-FENG. (**a**) Test photograph of the UST-FENG under positive electrode in the initial state. (**b**) Test photograph of the UST-FENG under reverse electrode in the initial state. (**c**) Open-circuit voltage diagram produced by the UST-FENG under stress. (**d**) After polarity switching, open-circuit voltage diagram produced by the UST-FENG under stress.

As a silicone rubber, Ecoflex not only possesses flexibility but also exhibits excellent tensile properties [23]. A tensile test was conducted on the UST-FENG using a tensile testing machine (SSBC-500, Kejun Inc., Suzhou, China). The initial and stretched states of the tested UST-FENG are shown in the inset in Figure 5a. The thickness and length of the tested UST-FENG were 0.8 mm and 50 mm, respectively. Figure 5a shows the stress–strain curve of the UST-FENG recorded by the universal testing machine. The results showed that the UST-FENG exhibited superior tensile capacity, with a fracture elongation rate of 574% and a stress at break of 1.34 MPa. The Young's modulus of the UST-FENG designed in this paper was relatively small, approximately 0.2 MPa. Its excellent tensile characteristics indicate its adaptability to a variety of wearable sensor application scenarios [38–40].

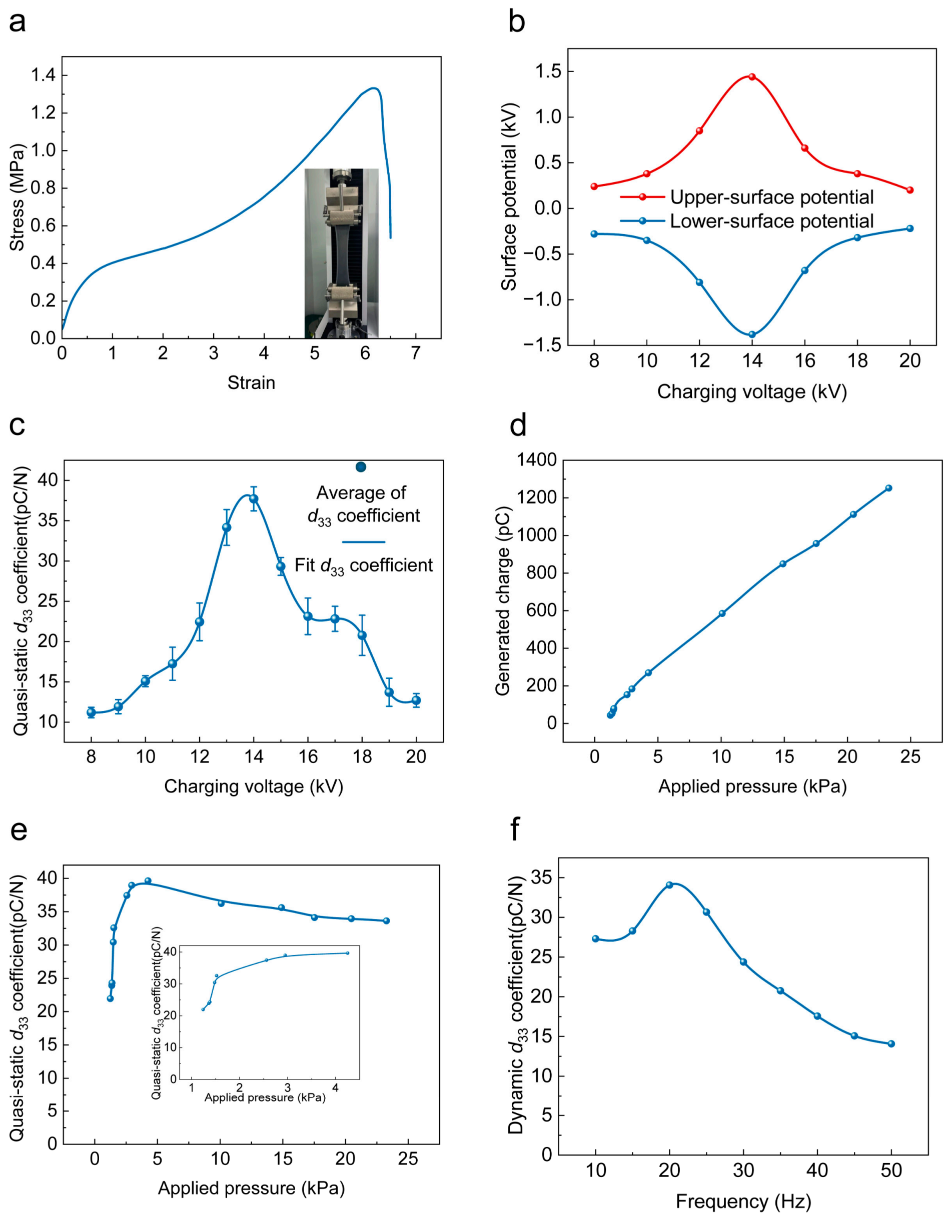

Figure 5. Characteristics of the UST-FENG. (**a**) Stress–strain curve of the UST-FENG. (**b**) Relationship diagram of the surface potential and charging voltage. (**c**) Relationship diagram of quasi-static d_{33} and charging voltage. (**d**) Relationship diagram of applied pressure and generated charge. (**e**) Relationship diagram of quasi-static d_{33} and applied pressure; the inset is the amplified diagram of the signal measured from 0 to 4.5 kPa. (**f**) Relationship diagram of dynamic d_{33} with frequency.

The piezoelectric properties of the UST-FENG were tested, providing data support for the targeted applications of the UST-FENG. The potential of the upper and lower surfaces of the UST-FENG was measured using a high-precision infrared electrostatic field meter (FMX-003, Tongrong Inc., Guangzhou, China). Figure 5b shows the effect of the charging voltage after polarization on the potential of the upper and lower surfaces of the UST-FENG. The results showed that when the charging voltage was 14 kV, the potentials of both the upper and lower surfaces of the UST-FENG reached their maximum values, being 1.44 kV and −1.38 kV, respectively. To assess the temporal stability of charge storage, we measured the surface potential over time. Over a 3-day period, we observed that the maximum surface potential reduced to 1.31 kV, a 9% reduction. This relatively small decrease in surface potential over this time frame indicates a good level of temporal stability for charge storage in our system. The piezoelectric signal generated by the UST-FENG was amplified by a charge amplifier (AFT-0966C, Love Volt Electronic Inc., Qinhuangdao, China) and then collected by a data acquisition card (DSO-2820, virtin). Figure 5c shows the relationship between the quasi-static d_{33} coefficient and the charging voltage. As shown in the figure, when the charging voltage is 14 kV, the quasi-static d_{33} coefficient of the UST-FENG reaches its maximum value of 38 pC/N, which coincides with the test results of the surface potential of the UST-FENG. Figure 5d shows the charge generated by the UST-FENG under a static load of 0~25 kPa. As the static load increases, the charge generated by the UST-FENG also increases, showing a positive correlation, indicating the good piezoelectric stability of the UST-FENG designed in this paper. Figure 5e shows the relationship between the quasi-static d_{33} and the pressure applied to the UST-FENG. It can be seen that as the load pressure increases, the quasi-static d_{33} coefficient first increases and then gradually decreases within the range of 25~40 pC/N. It is worth noting that in the range of lower load pressure (0–5 kPa), d_{33} rapidly increases, and then d_{33} tends to stabilize. The maximum d_{33} of approximately 39 pC/N is measured at 4 kPa. After multiple tests, the piezoelectric coefficient shows relative stability under various static and dynamic loads. The response of the d_{33} coefficient to the applied pressure can be attributed to the non-linear correlation between the Young's modulus and the inherent applied stress of the cell polymer material [14,41,42].

The dynamic piezoelectric characteristics of the UST-FENG were measured using an exciter (VT-50, YMC Piezotronics Inc., Yangzhou, China) to apply dynamic excitation force to the UST-FENG, and the acceleration was measured by an accelerometer (22A25, YMC Piezotronics Inc., Yangzhou, China). Figure 5f shows the relationship between the dynamic d_{33} and the frequency. As shown in the figure, the dynamic d_{33} first increases and then decreases in the range of 10 Hz to 50 Hz, with the maximum d_{33} of 34 pC/N at 20 Hz, and then sharply decreases at higher frequencies. It can be inferred that the resonance occurring at a vibration frequency of approximately 20 Hz leads to a significant increase in the longitudinal dynamic piezoelectric coefficient d_{33}. Compared with the static piezoelectric coefficient, the difference in the longitudinal dynamic piezoelectric coefficient is 10.53%, which can be attributed to the viscosity of Ecoflex as an organic silicone material [43,44].

4. Facial Muscle Detection

In recent years, interest in wearable device research has been increasing [38,44,45]. In this paper, a facial muscle detection device has been developed using a UST-FENG. The tiny movements of facial muscles when the face performs an action, such as blinking or speaking, allow the UST-FENG to be stressed and generate signals. The UST-FENG, based on intelligent motion-mechanics tape, offers exceptional flexibility, stretchability, and skin compatibility, ensuring comfortable adhesion to the skin of the face. The facial muscle movement signals recorded by the UST-FENG are also captured by a charge amplifier and a data acquisition card and then processed by a laptop. The transmission diagram of the UST-FENG-generated signal is shown in Figure 6a.

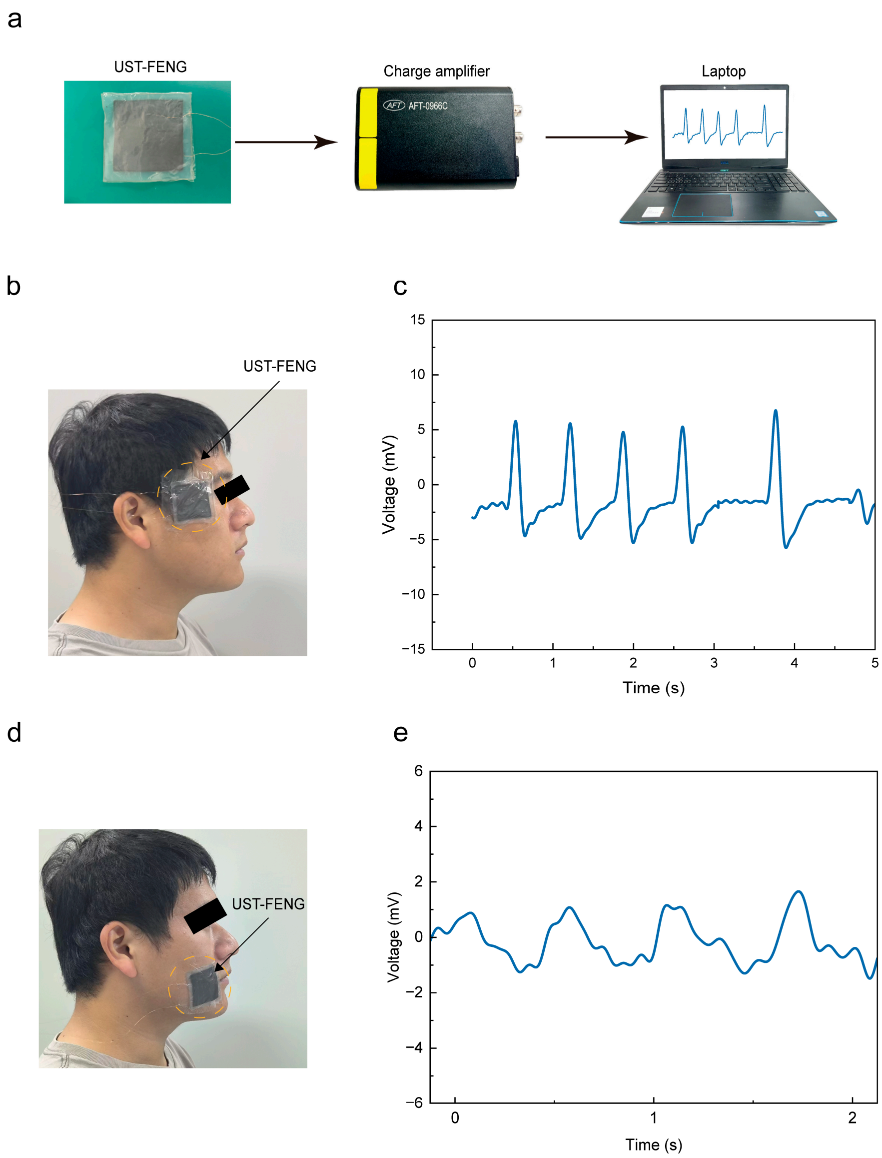

Figure 6. Application of the UST-FENG in the detection of facial muscle movement. (**a**) Transmission diagram of the UST-FENG-generated signal. (**b**) Photograph of the UST-FENG sticking on an eye. (**c**) Detection of blink signals by the UST-FENG. (**d**) Photograph of the UST-FENG sticking on a mouth. (**e**) Detection of speech signals by the UST-FENG.

Figure 6b shows the photograph of the UST-FENG sticking on an eye, and Figure 6c shows the blink signals detected by the UST-FENG. When the eyes are closed, the UST-FENG generates a negative signal, and when the eyes are open, the UST-FENG generates a positive signal. The amplitude and frequency of the signal correspond in real time with the amplitude and frequency of blinking. This device can assist stroke/paralysis patients who are unable to speak or move in conveying information, and it holds promise for detecting fatigue driving. Figure 6d shows the photograph of the UST-FENG sticking on a mouth, and Figure 6e shows the speech signals detected by the UST-FENG. When the mouth is open for speaking, UST-FENG generates a positive signal, and when the mouth is closed, the UST-FENG generates a reverse signal. The amplitude and frequency of the signal correspond in real time with the amplitude and frequency of mouth opening. This device can help aphonic patients convey information and holds potential for correcting people's poor speaking habits. Once the UST-FENG is integrated with a wireless transmission module and equipped with a dedicated mobile application for analyzing the captured data, it can provide effective and valuable insights about facial muscle information [46,47].

In the IoT scenario, electric energy should be produced on board by transforming ambient energy where and when available [48]. The UST-FENG is capable of generating electrical charges because of the piezoelectric effect. These generated charges can be utilized to drive the signal transmission process. By means of its internal energy, the UST-FENG can accomplish signal transmission without relying on external energy sources, thus being self-powered. To further evaluate the performance of this self-powered system, a test regarding power generation with the UST-FENG was carried out. It was measured that the UST-FENG generated an output power of 12 μW.

Overall, the UST-FENG represents a promising development in the field of facial wearable technology. With its remarkable sensitivity, high flexibility, high stretchability, and self-powered properties, it offers a multifunctional and potentially valuable tool for conveying information for the disabled and for facial muscle detection. As technology continues to evolve, it has the potential to transform the application scenarios of facial muscle detection sensors. Beyond its applications in conveying information for the disabled and facial muscle detection, the UST-FENG also has potential uses in other fields. For instance, it can be used to monitor the progress of patients recovering from facial muscle injuries. By tracking their facial muscle movements and providing feedback to therapists, the UST-FENG can help ensure patients receive the most effective treatment, contributing to innovative healthcare solutions.

5. Conclusions

This work, through the development of a UST-FENG designed for facial muscle recognition, has enriched the development of stretchable and soft self-powered ferroelectric nanogenerators. A series of experiments and performance evaluations were conducted in this paper, validating the mechanical performance and self-powered transmission capabilities of the UST-FENG. This confirmed its effectiveness and broad application potential. The UST-FENG developed in this study is based on the environmentally friendly, biodegradable, flexible material Ecoflex, which features controllable pore shape and density. Through simulation and experimentation, the piezoelectric properties of the UST-FENG were optimized. The experimental results show that the thickness of the UST-FENG is only 860 μm, the fracture elongation rate is as high as 574%, and the Young's modulus is only 0.2 MPa. Its quasi-static piezoelectric coefficient is approximately 38 pC/N. Further testing under various pressures and vibration frequencies confirmed its stability and reliability under both dynamic and quasi-static conditions, demonstrating that the UST-FENG has excellent thinness and superior stretchability. The use of this UST-FENG device not only identifies facial muscle movements, such as blinking and speaking, thereby helping to monitor people's facial conditions and improve their quality of life, but it can also be used to monitor the progress of patients recovering from facial muscle injuries. The successful application of the UST-FENG in facial muscle recognition opens up new avenues for the creation of intelligent motion sensors on the skin and robotic electronic skin.

Author Contributions: Writing—original draft preparation and Figure preparation, Z.S., X.C., Z.C., and Z.Z.; Writing—review and editing, Y.C. and W.L.; Project administration, W.L.; Funding acquisition, W.L. All authors have read and agreed to the published version of the manuscript.

Funding: This work was supported by the National Science Fund for Excellent Young Scholars of China (RK118QN23003), the Foundation of Jiangsu Specially-Appointed Professor, the Jiangsu Provincial Team of Innovation and Entrepreneurship (JSSCTD202351), Basic Science (Natural science) research project of higher education institutions in Jiangsu Province (24KJB460022), and the Natural Science Research Start-up Foundation of Nanjing University of Posts and Telecommunications (NY223124, NY223155).

Data Availability Statement: The data presented in this study are available on request from the corresponding author.

Conflicts of Interest: The authors declare no conflicts of interest.

References

1. Zhao, X.; Askari, H.; Chen, J. Nanogenerators for Smart Cities in the Era of 5G and Internet of Things. *Joule* **2021**, *5*, 1391–1431. [CrossRef]
2. Li, W.; Cao, Y.; Wang, C.; Sepúlveda, N. Ferroelectret Nanogenerators for the Development of Bioengineering Systems. *Cell Rep. Phys. Sci.* **2023**, *4*, 101388. [CrossRef]
3. Yang, Y. Multi-Effects Coupled Nanogenerators. *Nanoenergy Adv.* **2022**, *2*, 243–244. [CrossRef]
4. Qiu, X.; Bian, Y.; Liu, J.; Xiang, Y.; Ding, T.; Zhu, W.; Xuan, F.-Z. Ferroelectrets: Recent Developments. *IET Nanodielectr.* **2022**, *5*, 113–124. [CrossRef]
5. Owusu, F.; Venkatesan, T.R.; Nüesch, F.A.; Negri, R.M.; Opris, D.M. How to Make Elastomers Piezoelectric? *Adv. Mater. Technol.* **2023**, *8*, 2300099. [CrossRef]
6. Fang, P. Preparation and Investigation of Polymer-Foam Films and Polymer-Layer Systems for Ferroelectrets. Doctoral Dissertation, Universität Potsdam, Potsdam, Germany, 2010.
7. Li, W.; Torres, D.; Wang, T.; Wang, C.; Sepúlveda, N. Flexible and Biocompatible Polypropylene Ferroelectret Nanogenerator (FENG): On the Path toward Wearable Devices Powered by Human Motion. *Nano Energy* **2016**, *30*, 649–657. [CrossRef]
8. Li, W.; Wu, N.; Zhong, J.; Zhong, Q.; Zhao, S.; Wang, B.; Cheng, X.; Li, S.; Liu, K.; Hu, B.; et al. Theoretical Study of Cellular Piezoelectret Generators. *Adv. Funct. Mater.* **2016**, *26*, 1964–1974. [CrossRef]
9. Wan, X.; Chen, P.; Xu, Z.; Mo, X.; Jin, H.; Yang, W.; Wang, S.; Duan, J.; Hu, B.; Luo, Z.; et al. Hybrid-Piezoelectret Based Highly Efficient Ultrasonic Energy Harvester for Implantable Electronics. *Adv. Funct. Mater.* **2022**, *32*, 2200589. [CrossRef]
10. Moreira, M.M.A.C.; Soares, I.N.; Assagra, Y.A.O.; Sousa, F.S.I.; Nordi, T.M.; Dourado, D.M.; Gounella, R.H.; Carmo, J.P.; Altafim, R.A.C.; Altafim, R.A.P. Piezoelectrets: A Brief Introduction. *IEEE Sens. J.* **2021**, *21*, 22317–22328. [CrossRef]
11. Qiu, X. Patterned Piezo-, Pyro-, and Ferroelectricity of Poled Polymer Electrets. *J. Appl. Phys.* **2010**, *108*, 011101. [CrossRef]
12. Sodhi, T.K.; Chrétien, P.; Bui, Q.C.; Chevillard, A.; Travers, L.; Morassi, M.; Tchernycheva, M.; Houzé, F.; Gogneau, N. Surface Charge: An Advantage for the Piezoelectric Properties of GaN Nanowires. *Nanoenergy Adv.* **2024**, *4*, 133–146. [CrossRef]
13. Shi, J.; Zhu, D.; Beeby, S.P. An Investigation of PDMS Structures for Optimized Ferroelectret Performance. *J. Phys. Conf. Ser.* **2014**, *557*, 012104. [CrossRef]
14. Fang, P.; Wegener, M.; Wirges, W.; Gerhard, R.; Zirkel, L. Cellular Polyethylene-Naphthalate Ferroelectrets: Foaming in Supercritical Carbon Dioxide, Structural and Electrical Preparation, and Resulting Piezoelectricity. *Appl. Phys. Lett.* **2007**, *90*, 192908. [CrossRef]
15. Zirkel, L.; Jakob, M.; Münstedt, H. Foaming of Thin Films of a Fluorinated Ethylene Propylene Copolymer Using Supercritical Carbon Dioxide. *J. Supercrit. Fluids* **2009**, *49*, 103–110. [CrossRef]
16. Perna, G.; Bonacci, F.; Caponi, S.; Clementi, G.; Michele, A.D.; Gammaitoni, L.; Mattarelli, M.; Neri, I.; Puglia, D.; Cottone, F. 3D-Printed Piezoelectret Based on Foamed Polylactic Acid for Energy-Harvesting and Sensing Applications. *Nanomaterials* **2023**, *13*, 2953. [CrossRef]
17. Palitó, T.T.C.; Assagra, Y.A.O.; Altafim, R.A.P.; Carmo, J.P.; Altafim, R.A.C. Hydrophone Based on 3D Printed Polypropylene (PP) Piezoelectret. *Electron. Lett.* **2019**, *55*, 203–204. [CrossRef]
18. Seggern, H.; Zhukov, S.; Fedosov, S. Poling Dynamics and Thermal Stability of FEP/ePTFE/FEP Sandwiches. *IEEE Trans. Dielectr. Electr. Insul.* **2010**, *17*, 1056–1065. [CrossRef]
19. Zhang, X.; Huang, J.; Chen, J.; Wan, Z.; Wang, S.; Xia, Z. Piezoelectric Properties of Irradiation-Crosslinked Polypropylene Ferroelectrets. *Appl. Phys. Lett.* **2007**, *91*, 182901. [CrossRef]
20. Pastrana, J.; Dsouza, H.; Cao, Y.; Figueroa, J.; González, I.; Vilatela, J.J.; Sepúlveda, N. Electrode Effects on Flexible and Robust Polypropylene Ferroelectret Devices for Fully Integrated Energy Harvesters. *ACS Appl. Mater. Interfaces* **2020**, *12*, 22815–22824. [CrossRef]
21. Zhong, J.; Ma, Y.; Song, Y.; Zhong, Q.; Chu, Y.; Karakurt, I.; Bogy, D.B.; Lin, L. A Flexible Piezoelectret Actuator/Sensor Patch for Mechanical Human-Machine Interfaces. *ACS Nano* **2019**, *13*, 7107–7116. [CrossRef]
22. Kumar, K.A.; Sreekala, M.S.; Arun, S. Studies on Properties of Bio-Composites from Ecoflex/Ramie Fabric-Mechanical and Barrier Properties. *J. Biomater. Nanobiotechnol.* **2012**, *3*, 396–404. [CrossRef]
23. Del Bosque, A.; Sánchez-Romate, X.F.; Gómez, A.; Sánchez, M.; Ureña, A. Highly Stretchable Strain Sensors Based on Graphene Nanoplatelet-Doped Ecoflex for Biomedical Purposes. *Sens. Actuators Phys.* **2023**, *353*, 114249. [CrossRef]
24. Tang, X.; Dong, Y.; Li, Q.; Liu, Z.; Yan, N.; Li, Y.; Liu, B.; Jiang, L.; Song, R.; Wang, Y.; et al. Using Microneedle Array Electrodes for Non-Invasive Electrophysiological Signal Acquisition and Sensory Feedback Evoking. *Front. Bioeng. Biotechnol.* **2023**, *11*, 1238210. [CrossRef] [PubMed]
25. Fu, J.; Huang, S.; Cao, J.; Huang, J.; Xu, D.; Jiang, N.; Li, X.; Li, G.; Fang, P. Microneedle Array Electrodes Fabricated With 3D Printing Technology for High-Quality Electrophysiological Acquisition. *IEEE Trans. Neural Syst. Rehabil. Eng.* **2024**, *32*, 2460–2469. [CrossRef] [PubMed]
26. Jiang, N.; Wang, L.; Wang, D.; Fang, P.; Wu, X.; Li, G. Loading Recognition for Lumbar Exoskeleton Based on Multi-Channel Surface Electromyography From Low Back Muscles. *IEEE Trans. Biomed. Eng.* **2024**, *71*, 2154–2162. [CrossRef]
27. Lamberti, A.; Clerici, F.; Fontana, M.; Scaltrito, L. A Highly Stretchable Supercapacitor Using Laser-Induced Graphene Electrodes onto Elastomeric Substrate. *Adv. Energy Mater.* **2016**, *6*, 1600050. [CrossRef]

28. Lin, Z.; Kireev, D.; Liu, N.; Gupta, S.; LaPiano, J.; Obaid, S.N.; Chen, Z.; Akinwande, D.; Efimov, I.R. Graphene Biointerface for Cardiac Arrhythmia Diagnosis and Treatment. *Adv. Mater.* **2023**, *35*, 2212190. [CrossRef]
29. Shen, Q.; Jiang, M.; Wang, R.; Song, K.; Vong, M.H.; Jung, W.; Krisnadi, F.; Kan, R.; Zheng, F.; Fu, B.; et al. Liquid Metal-Based Soft, Hermetic, and Wireless-Communicable Seals for Stretchable Systems. *Science* **2023**, *379*, 488–493. [CrossRef]
30. Ma, X.; Song, C.; Zhang, F.; Dai, Y.; He, P.; Zhang, X. Soft, Multifunctional, Robust Film Sensor Using a Ferroelectret with Significant Longitudinal and Transverse Piezoelectric Activity for Biomechanical Monitoring. *ACS Appl. Mater. Interfaces* **2022**, *14*, 51291–51300. [CrossRef]
31. Aguilar, J.Q.; Muñoz, M.; Álvarez-Arenas, T.G. Interpretation of the Thickness Resonances in Ferroelectret Films Based on a Layered Sandwich Mesostructure and a Cellular Microstructure. *IEEE Trans. Ultrason. Ferroelectr. Freq. Control* **2021**, *68*, 1245–1252. [CrossRef]
32. Cao, Y.; Figueroa, J.; Li, W.; Chen, Z.; Wang, Z.L.; Sepúlveda, N. Understanding the Dynamic Response in Ferroelectret Nanogenerators to Enable Self-Powered Tactile Systems and Human-Controlled Micro-Robots. *Nano Energy* **2019**, *63*, 103852. [CrossRef]
33. Kumar, A.; Saini, D.; Mandal, D. 3D Printed Ferroelectret with Giant Piezoelectric Coefficient. *Appl. Phys. Lett.* **2022**, *120*, 182901. [CrossRef]
34. Mo, X.; Zhou, H.; Li, W.; Xu, Z.; Duan, J.; Huang, L.; Hu, B.; Zhou, J. Piezoelectrets for Wearable Energy Harvesters and Sensors. *Nano Energy* **2019**, *65*, 104033. [CrossRef]
35. Qiu, X. Polymer Electrets and Ferroelectrets as EAPs: Materials. In *Electromechanically Active Polymers: A Concise Reference*; Carpi, F., Ed.; Polymers and Polymeric Composites: A Reference Series; Springer International Publishing: Cham, Switzerland, 2016; pp. 561–589, ISBN 978-3-319-31530-0.
36. Li, X.; Wang, Y.; Xu, M.; Shi, Y.; Wang, H.; Yang, X.; Ying, H.; Zhang, Q. Polymer Electrets and Their Applications. *J. Appl. Polym. Sci.* **2021**, *138*, 50406. [CrossRef]
37. Wegener, M.; Bauer, S. Microstorms in Cellular Polymers: A Route to Soft Piezoelectric Transducer Materials with Engineered Macroscopic Dipoles. *ChemPhysChem* **2005**, *6*, 1014–1025. [CrossRef]
38. Wang, N.; Daniels, R.; Connelly, L.; Sotzing, M.; Wu, C.; Gerhard, R.; Sotzing, G.A.; Cao, Y. All-Organic Flexible Ferroelectret Nanogenerator with Fabric-Based Electrodes for Self-Powered Body Area Networks. *Small* **2021**, *17*, 2103161. [CrossRef]
39. Miriyev, A.; Stack, K.; Lipson, H. Soft Material for Soft Actuators. *Nat. Commun.* **2017**, *8*, 596. [CrossRef]
40. Shi, J.; Beeby, S. Textiles Based Ferroelectret Generator with Enhanced Energy Harvesting Performance. In Proceedings of the 2020 IEEE International Conference on Flexible and Printable Sensors and Systems (FLEPS), Manchester, UK, 16–19 August 2020; pp. 1–4. [CrossRef]
41. Zhong, J.; Zhong, Q.; Zang, X.; Wu, N.; Li, W.; Chu, Y.; Lin, L. Flexible PET/EVA-Based Piezoelectret Generator for Energy Harvesting in Harsh Environments. *Nano Energy* **2017**, *37*, 268–274. [CrossRef]
42. Ploner, M.; Wang, N.; Wu, C.; Daniels, R.; Huo, J.; Sotzing, G.A.; Cao, Y. Ultrathin, All-Organic, Fabric-Based Ferroelectret Loudspeaker for Wearable Electronics. *iScience* **2022**, *25*, 105607. [CrossRef]
43. Zhou, Y.; Zhao, X.; Xu, J.; Fang, Y.; Chen, G.; Song, Y.; Li, S.; Chen, J. Giant Magnetoelastic Effect in Soft Systems for Bioelectronics. *Nat. Mater.* **2021**, *20*, 1670–1676. [CrossRef]
44. Zhao, X.; Zhou, Y.; Xu, J.; Chen, G.; Fang, Y.; Tat, T.; Xiao, X.; Song, Y.; Li, S.; Chen, J. Soft Fibers with Magnetoelasticity for Wearable Electronics. *Nat. Commun.* **2021**, *12*, 6755. [CrossRef] [PubMed]
45. Pu, X.; An, S.; Tang, Q.; Guo, H.; Hu, C. Wearable Triboelectric Sensors for Biomedical Monitoring and Human-Machine Interface. *iScience* **2021**, *24*, 102027. [CrossRef] [PubMed]
46. Park, S.; Thangavel, G.; Parida, K.; Li, S.; Lee, P.S. A Stretchable and Self-Healing Energy Storage Device Based on Mechanically and Electrically Restorative Liquid-Metal Particles and Carboxylated Polyurethane Composites. *Adv. Mater.* **2019**, *31*, 1805536. [CrossRef] [PubMed]
47. Zhang, X.; Hillenbrand, J.; Sessler, G.M. Ferroelectrets with Improved Thermal Stability Made from Fused Fluorocarbon Layers. *J. Appl. Phys.* **2007**, *101*, 054114. [CrossRef]
48. Clementi, G.; Cottone, F.; Di Michele, A.; Gammaitoni, L.; Mattarelli, M.; Perna, G.; López-Suárez, M.; Baglio, S.; Trigona, C.; Neri, I. Review on Innovative Piezoelectric Materials for Mechanical Energy Harvesting. *Energies* **2022**, *15*, 6227. [CrossRef]